electronic reprint

JOURNAL OF APPLIED CRYSTALLOGRAPHY

ISSN: 1600-5767

journals.iucr.org/j

Crystallographic orientation relationships in the $\alpha \rightarrow \gamma'$ martensitic transformation in an Fe–Mn–Al–Ni system

Juan Manuel Vallejos, César Enrique Sobrero, Martina Ávalos, Javier Walter Signorelli and Jorge Alberto Malarría

J. Appl. Cryst. (2018). **51**, 990–997

JOURNAL OF APPLIED CRYSTALLOGRAPHY
ISSN 1600-5767

Crystallographic orientation relationships in the $\alpha \rightarrow \gamma'$ martensitic transformation in an Fe–Mn–Al–Ni system

Juan Manuel Vallejos,[a,b,c]* César Enrique Sobrero,[a,b] Martina Ávalos,[a,b] Javier Walter Signorelli[a,b] and Jorge Alberto Malarría[a,b]

[a]Instituto de Física Rosario, Universidad Nacional de Rosario – CONICET, Bv. 27 de febrero 210 bis, Rosario, Santa Fe 2000, Argentina, [b]Facultad de Ciencias Exactas, Ingeniería y Agrimensura, Universidad Nacional de Rosario, Pellegrini 250, Rosario, Santa Fe 2000, Argentina, and [c]Facultad de Ingeniería, Universidad Nacional del Nordeste, Las Heras 727, Resistencia, Chaco H3500, Argentina. *Correspondence e-mail: vallejos@ifir-conicet.gov.ar

Received 9 October 2017
Accepted 2 May 2018

Edited by G. Kostorz, ETH Zurich, Switzerland

Keywords: shape-memory alloys (SMAs); martensitic phase transformations; orientation imaging microscopy (OIM); orientation relationships.

The $Fe_{43.5}Mn_{34}Al_{15}Ni_{7.5}$ (at.%) alloy exhibits outstanding pseudoelastic behaviour over a wide range of temperatures. This alloy undergoes an unusual martensitic transformation from a disordered body-centred cubic (α) parent phase to a face-centred cubic (γ') product phase. In the present work, the orientations of the parent and product phases for quenched samples were analysed by electron backscatter diffraction. Bain, Kurdjumow–Sachs, Pitsch, Nishiyama–Wassermann and Greninger–Troiano orientation relationships between the parent and product phases were compared with experimental results. The Pitsch relationship appears to be the most suitable to describe the $\alpha \rightarrow \gamma'$ martensitic transformation. This result provides experimental support to the dislocation-based heterogeneous Bogers–Burgers type transformation mechanism. No indications of variant selection were detected in the thermally activated transformations.

1. Introduction

Martensitic phase transitions have been found in several metallic systems (Nishiyama, 1978). The formation of this phase involves the coordinated movement of atoms without diffusion (Roitburd & Kurdjumov, 1979). As a consequence, there is a crystallographic relationship between the lattice of the parent phase (austenite) and the product phase (martensite), usually referred to as an orientation relationship (OR). The OR indicates a correspondence between the planes and directions of the parent and product phases.

The first model proposed to explain the martensitic transformation in steels was developed by Bain (1924), abbreviated herein as B. In that work, it was proposed that an intermediate tetragonal lattice (body-centred tetragonal, b.c.t.) is formed from the face-centred cubic (f.c.c., γ) lattice by choosing the directions $\frac{1}{2}[110]_\gamma$, $\frac{1}{2}[\bar{1}10]_\gamma$ and $[001]_\gamma$ as the new frame of reference. Expanding the first two vectors and reducing the third one, a body-centred cubic (b.c.c., α') lattice with the appropriate parameters is obtained. Because of the symmetry of the f.c.c. phase, it is possible to choose the major axis of the b.c.t. lattice in three orthogonal directions ($\langle 100 \rangle_\gamma$). Therefore, a parent-phase crystal can be transformed into three different product-phase variants, as shown in Fig. 1. Although this OR was actually never found in steels, it is used as the first approximation when studying the transformation $\gamma \rightarrow \alpha'$.

A different model, focused on explaining the OR determined by X-ray diffraction measurements, was proposed by

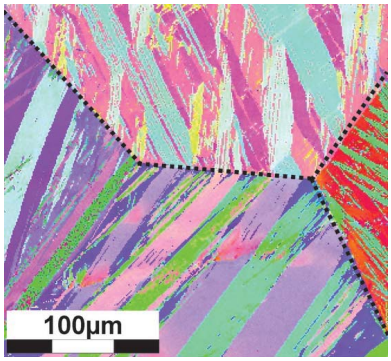

Kurdjumow & Sachs (1930), abbreviated herein as KS. These authors found that, in high-carbon steels, the planes and directions defined by Bain are not exactly parallel. These results were later supported by studies by different researchers (Nishiyama, 1934; Wassermann, 1935; Pitsch, 1959; Greninger & Troiano, 1949). In some cases, differences of several degrees were reported between crystallographic orientations. On the basis of these divergences, KS developed a new model that relates the compact planes of the γ phase to those of the α' phase ($\{111\}_\gamma \parallel \{110\}_{\alpha'}$) and the compact directions of these planes ($\langle 110\rangle_\gamma \parallel \langle 111\rangle_{\alpha'}$). The martensite lattice is generated from an f.c.c. parent lattice by a shear on $\{111\}_\gamma$ planes along $\langle 110\rangle_\gamma$ directions. Thus, the planes and directions that remain parallel within the f.c.c. structure are those that form the slip systems. The number of possible martensite variants can be defined using the four planes of the family $\{111\}_\gamma$ and the three directions $\langle 110\rangle_\gamma$ corresponding to each of these planes. Since both $\langle 110\rangle_\gamma$ directions and their opposites can be chosen, 24 variants are possible in this model. In 1934, on the basis of observations made on nickel steels, Nishiyama (1934) proposed a model very similar to that described above. This OR has the same parallel planes as the KS model, but with the direction $[10\bar{1}]_\gamma$ parallel to $[100]_{\alpha'}$. In this case, the shear occurs on $\{111\}_\gamma$ planes along $\langle 112\rangle_\gamma$ directions. A year later, Wassermann (1935) independently postulated the same relationship as Nishiyama. This OR is thus known as Nishiyama–Wassermann (NW). One of these two relationships is usually found in the martensitic transformation of steels.

Besides the KS and NW ORs, several models to explain the $\gamma\rightarrow\alpha'$ transformation have been proposed since then. Pitsch (1959) (abbreviated herein as P) established an OR for the martensitic transformation in Fe–N alloys by transmission electron microscopy (TEM) observations. This relationship was observed between perlite, ferrite and cementite phases in steels (Pitsch, 1962). The Pitsch OR relates $\{0\bar{1}1\}_\alpha \parallel \{001\}_\gamma$ planes and $\langle 111\rangle_\alpha \parallel \langle 110\rangle_\gamma$ directions. Later, Bogers & Burgers (1964) proposed a homogeneous double-shear mechanism for the $\gamma\rightarrow\alpha$ transformation. This model yields different relationships between these phases, depending on the misfit dislocations generated at interfaces to release misfit strains (Yang *et al.*, 2014).

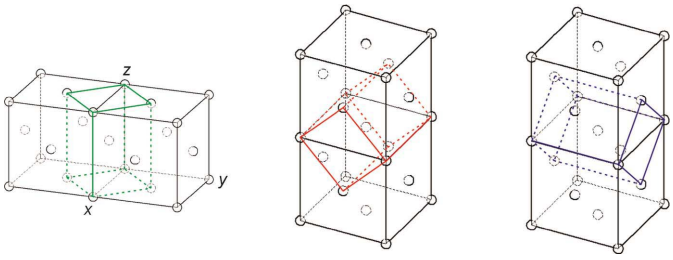

Figure 1
Bain's lattice correspondence. The lattice points in the f.c.c. parent phase are uniquely related on a one-to-one basis to those in the b.c.t. product phase. The major axis of the three b.c.t. product phases corresponds to three $\langle 100\rangle_\gamma$ orthogonal directions of the parent phase. As a consequence, three crystallographic orientations of the product phase are possible, corresponding to each of the three variants of martensite by the Bain model.

Although the KS and NW models can predict the orientations of the product phases in most steels, the habit planes calculated from these ORs do not correspond to those measured in some materials (Greninger & Troiano, 1949). Also, Greninger and Troiano (GT) based their criticisms of these models on the large movements and adjustments for lattice transformation. They proposed a two-homogeneous-shear mechanism for the $\gamma\rightarrow\alpha$ transformation: the first is responsible for the macroscopically observed change in shape, while the second is needed to complete the changes in the crystal structure without macroscopic consequences. Unlike the previous ones, this OR cannot be expressed by a low-index representation $\{hkl\}\langle uvw\rangle$ type. The GT model is used to represent the crystallographic relationship between austenite and granular bainite in some steels. The development of this mechanism led to the phenomenological theory of martensitic transformation (Wechsler *et al.*, 1953; Bowles & Mackenzie, 1954*a*,*b*; Mackenzie & Bowles, 1954).

A lattice transformation represents a transition from one crystal lattice to another. When the aim of a study is related to the rotation between lattices, it is only necessary to bring the coordinate systems of the parent and product phases into coincidence. For this purpose, only the rotation matrix component of the transformation matrix is needed.

There are several ways to represent an OR. The minimum rotation around an invariant line representation and the Euler angles representation are two of the most common. The former is generally described using a rotation axis (d) and a rotation angle (ω). The latter uses three rotations (φ_1, Φ and φ_2) to bring the parent- and product-phase coordinate systems into coincidence.

Atomistic calculations showed that the NW distortion is more energetically favourable for the $\gamma\rightarrow\alpha'$ martensitic transformation than the ones proposed by Bain (Sandoval *et al.*, 2009). Similar results were obtained by Ojha & Sehitoglu (2016), who studied the transformation between the parent b.c.c. phase (α) and the product f.c.c. phase (γ') in the Fe–Mn–Al–Ni (FMAN) system. They proposed a dislocation-based heterogeneous Bogers–Burgers-type transformation mechanism that proceeds with a much lower energy barrier than that involved in the Bain model.

Recent studies suggest that the $\gamma\rightarrow\alpha'$ martensitic transformation is a result of a $\gamma\rightarrow\varepsilon\rightarrow\alpha'$ two-step mechanism (where ε is an intermediate hexagonal phase) (Cayron *et al.*, 2010). This theory implies a gradual reorientation of the martensite variants during their growth in the deformed austenite lattice as a consequence of the transformation itself (Cayron, 2013; Yang *et al.*, 2014; Sinclair & Hoagland, 2008). This theory could explain why the ORs observed in martensitic transformations differ depending on the material.

The appearance of one OR to the detriment of the others is indicative of the specific coordinate atomic displacements that transform one lattice into another and thus provides a direct clue to the transformation mechanism. A summary of all the crystallographic ORs described above is presented in Table 1.

Table 1
Summary of the five OR models used.

B, KS, P, NW and GT represent the Bain, Kurdjumow–Sachs, Pitsch, Nishiyama–Wassermann and Greninger–Troiano ORs, respectively. The corresponding crystallographic parallel planes and directions in the two phases describing the α/γ interfaces for each model are shown. The Euler angle representation and the number of martensite variants for each model are also presented.

OR	Planes	Directions	Transformation Euler angles ($\gamma\rightarrow\alpha$)			No. of martensite variants
			φ_1 (°)	Ψ (°)	φ_2 (°)	
B	$\{010\}_\gamma \parallel \{010\}_\alpha$	$\langle 001\rangle_\gamma \parallel \langle 101\rangle_\alpha$	0	45	0	3
KS	$\{111\}_\gamma \parallel \{110\}_\alpha$	$\langle 1\bar{1}0\rangle_\gamma \parallel \langle 1\bar{1}1\rangle_\alpha$	5.77	48.2	5.77	24
P	$\{001\}_\gamma \parallel \{\bar{1}01\}_\alpha$	$\langle 110\rangle_\gamma \parallel \langle 111\rangle_\alpha$	9.74	45	0	12
NW	$\{111\}_\gamma \parallel \{110\}_\alpha$	$\langle 0\bar{1}1\rangle_\gamma \parallel \langle 001\rangle_\alpha$	0	45	9.74	12
GT	$\{111\}_\gamma \sim 1^\circ$ to $\{110\}_\alpha$	$\langle \bar{1}2\bar{1}\rangle_\gamma \sim 2^\circ$ to $\langle 1\bar{1}0\rangle_\alpha$	2.7	46.6	7.5	24

The relationships between planes and directions shown for the GT model are approximate. Further information about these ORs is given by Nolze (2004).

The martensitic transformations can be induced, depending on the alloy, either thermally or by the application of mechanical stress (Nishiyama, 1978). If the product phase is induced by mechanical stress and the parent phase is recovered by unloading the material, it is said that the alloy has a pseudoelastic response (Otsuka, 2002). The alloys with the greatest number of applications are Ni–Ti alloys and Cu-based alloys. However, NiTi production costs are high and its cold workability is very poor. Cu-based alloys have their drawbacks related to phase stability (Ahlers, 1986), and may be brittle in polycrystalline form (Sure & Brown, 1984). For this reason, Fe-based shape-memory alloys (SMAs) were developed in the search for good candidates to overcome the disadvantages of classical SMAs. Nevertheless, traditional Fe-based SMAs exhibit poor pseudoelastic recovery (Sato *et al.*, 1982; Sehitoglu *et al.*, 2001; Ando *et al.*, 2009).

The recently discovered alloy $Fe_{43.5}Mn_{34}Al_{15}Ni_{7.5}$ (at.%) exhibits impressive pseudoelastic behaviour over a wide range of temperatures (Omori *et al.*, 2011). This feature is attractive for automotive, space, cryogenic and seismic applications. The alloy undergoes an unusual martensitic transformation from a disordered b.c.c. parent phase to an f.c.c. product phase (Omori *et al.*, 2011; Umino *et al.*, 2006). The appearance of coherent B2-ordered Ni-rich precipitates in the disordered b.c.c. matrix produces a thermoelastic transformation in the alloy. Tseng *et al.* (2015) studied the pseudoelastic response of an FMAN single crystal oriented in the $[100]_\alpha$ direction under tension and compression loads. The good shape recovery of the material under compression was attributed to the fact that, in this stress configuration, two martensite variants can be activated according to the Bain model. On the other hand, the poor recovery in tension could be because only one martensite variant can assist the deformation in this state of stress, which has more difficulty in accommodating the geometric incompatibilities produced during deformation.

The crystallographic orientation of the crystals has an enormous influence on the shape-memory properties of this alloy, both in bamboo-like and monocrystalline structures (Tseng *et al.*, 2016; Vollmer *et al.*, 2016). Tseng *et al.* (2016) analysed the strain recovery in FMAN single crystals oriented in the $[100]_\alpha$ and $[123]_\alpha$ directions. Although the theoretical calculations yield greater deformation associated with the phase transformation in the $[100]_\alpha$ direction, the experimental results established a greater recovery in the $[123]_\alpha$ direction. The degradation of the pseudoelastic response of two samples with bamboo-like microstructures, oriented in directions $[001]_\alpha$ and $[409]_\alpha$, was studied by Vollmer *et al.* (2016). In both samples there was an early degradation of the pseudoelastic response and a high density of dislocations was observed. However, the decrease in pseudoelastic recovery was faster in the sample oriented in the $[409]_\alpha$ direction.

The $\gamma\rightarrow\alpha'$ martensitic transformation has been extensively studied since Bain's seminal paper. However, the mechanism of variant selection in the $\alpha\rightarrow\gamma'$ transformation of the Fe–Mn–Al system is not fully understood at present. In addition, the incompatibilities between the parent and product lattices generated by this transformation have not been explained in detail. Although some considerations of the classical models can be used to approach these problems, the features of this transformation must be studied in a particular way. This is necessary in order to optimize the pseudoelastic properties of the FMAN system. In the present work, the crystallographic OR generated in the martensitic transformation of this system was studied systematically. Five ORs (B, KS, P, NW and GT) were assessed in order to study the correspondence between the experimental results of the orientations measured by electron backscatter diffraction (EBSD) and the ideal orientations. Thus, we sought to contribute to the discussion of the $\alpha\rightarrow\gamma'$ transformation produced in this alloy. The identification of ORs in this material is fundamental to the study of its martensitic transformation in order to approach the problem of variant selection, generation of favourable textures for shape-memory recovery and numerical modelling of the pseudoelastic behaviour.

2. Methodology

2.1. Material development and crystallographic orientation measurement

$Fe_{43.5}Mn_{34}Al_{15}Ni_{7.5}$ (at.%, nominal composition) was melted in an arc furnace and then homogenized under an argon atmosphere at 1273 K for 24 h. Then, the alloy was

hot-rolled at 1273 K to a thickness of 1.1 mm with a total deformation of 87.5%. Specimens of 1.5 × 1.5 mm were cut with a diamond saw. Finally, the samples were encapsulated in quartz tubes under vacuum, annealed for 1 h at 1523 K, and then water quenched at room temperature by breaking the capsules. As a result of quenching, the high-temperature b.c.c. structure partially transforms to martensite.

The samples were examined with an FEI QUANTA 200 scanning electron microscope equipped with a field-emission gun (Thermo Fisher Scientific) with the *OIM Data Collection* and *Analysis* software (version 5.31; EDAX, Mahwah, NJ, USA) and an orientation imaging microscopy–EBSD detector system. The EBSD detector is an EDAX TSLOIM, with a phosphor screen and a DigiView CCD camera. For EBSD mapping the specimens were prepared using mechanical polishing techniques. The polishing steps included diamond pastes of 9, 6, 3 and 1 µm. The process was finished using 0.05 µm colloidal silica for 10 min. For the final polishing, ethyleneglycol instead of water was used as lubricant to prevent oxidation of the surface. Low force and a wheel rotation of 100 r min^{-1} were used to avoid martensitic transformation by the polishing procedure. The step sizes selected for the maps were from 0.2 to 0.07 µm, depending on the microstructural features such as grain and martensite plate sizes. The orientations of all the martensite variants observed in 32 b.c.c. grains were measured by EBSD, as well as the orientations of the austenitic phases. In total, 44 different martensite variants were processed in these grains.

2.2. Rotation matrices, ideal orientations and misorientation angle calculations

The lattice transformation is a transition from one crystal lattice into another and it is represented by a transformation matrix. As the aim of this paper is to evaluate the orientation between the α and γ' lattices and not the lattice strains, only the rotation matrix component of the transformation matrix is needed. The base rotation matrix (OR_1) of each ideal relationship was calculated from the Euler angles defined for the transformation $\gamma \rightarrow \alpha$, shown in Table 1. In order to obtain all the rotational matrices of each OR, we used the group of 24 rotations ($\mathbf{P}_i$) that describes the symmetry of cubic crystals, summarized by Koumatos & Muehlemann (2017). Equation (1) was used to perform these calculations:

$$OR_i = (OR_1)(\mathbf{P}_i). \quad (1)$$

Consequently, for each $i = 1, \ldots, 24$, the corresponding rotation matrix (OR_i) was calculated according to the ideal OR. The rotation produced by the matrix $\mathbf{P}_1$, being the identity, generates the same OR_1. Owing to the cubic symmetry, in the B, P and NW models some of the 24 rotation matrices are symmetrically equivalent. Only three matrices for the first model and 12 matrices for the last two represent independent rotations.

Because both parent and product phases present a cubic crystal symmetry, each crystallographic orientation of any of these phases can be defined in 24 symmetrically equivalent different ways. In order to establish a criterion to identify uniquely which martensite variant is activated inside a parent grain, all the orientations measured by EBSD were converted to their expression in the fundamental region. In this zone there is a one-to-one relationship between a particular orientation of the cubic crystal and its expression in Euler angles. Similar methodologies to identify variant selection were used in some previous studies (He *et al.*, 2005; Verbeken *et al.*, 2009).

The average values of the crystallographic orientations of both the martensite variants and the austenite grains were calculated using the *MTEX* software (Hielscher & Schaeben, 2008). All possible ideal orientations of the parent phase that establish the models for each variant of the product phase were calculated using equation (2). We also determined which of the ideal variants best matches the measured parent-phase orientation. For this purpose, the misorientation angle between each one of these ideal parent-phase orientations and the orientations measured by EBSD was obtained:

$$\mathbf{M}_i^{\text{b.c.c.}} = (OR_i)(\mathbf{M}^{\text{f.c.c.}}), \quad (2)$$

with i from 1 to 3 for B, 1 to 24 for KS and GT, and 1 to 12 for P and NW. $\mathbf{M}_i^{\text{b.c.c.}}$ represents the orientation matrix of an ideal parent phase according to the model and $\mathbf{M}^{\text{f.c.c.}}$ represents the orientation matrix of a product-phase variant measured by EBSD.

3. Results and discussion

Scanning electron microscopy (SEM) and inverse pole figure (IPF) images showing 3 of the 32 analysed b.c.c. grains are shown in Figs. 2(*a*) and 2(*b*), respectively. The orientations of different product phases can be observed. For grain 1 there are four different variants of martensite, whereas for grains 2 and 3 only three and two variants were found, respectively. Table 2 summarizes the number of b.c.c. grains with one, two, three or four martensite variants activated. In most of the measured grains (not all shown, for the sake of simplicity), only one or two martensite variants were observed. Fig. 3(*a*) gives $(011)_\alpha$ and $(111)_\alpha$ pole figures showing the crystal average orientations of the 32 b.c.c. grains measured by EBSD. The reconstructed pole figures show the typical components of a

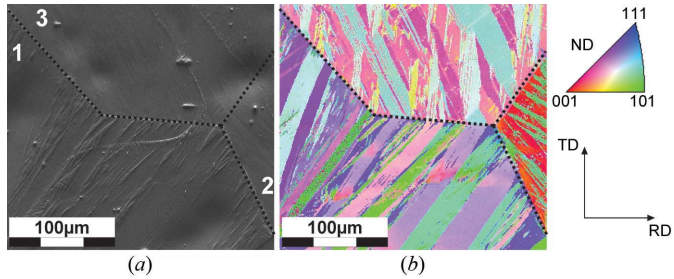

Figure 2
(*a*) SEM image of b.c.c. grains 1, 2 and 3. (*b*) IPF image showing the crystal orientations in the same grains. ND, RD and TD represent the out-of-plane, rolling and transverse directions of the sample, respectively. Dashed lines correspond to grain boundaries. The step size is 0.3 µm.

Table 2
Summary of the number of martensite variants found in the b.c.c. grains measured.

Number of martensite variants in the b.c.c. grain	Number of b.c.c. grains
1	23
2	7
3	1
4	1

hot-rolled b.c.c. texture. The $(001)_\gamma$ and $(011)_\gamma$ pole figures are plotted in Fig. 3(*b*), showing the 44 f.c.c. crystal average orientations. The correspondence between these two pole figures and $(011)_\alpha$ and $(111)_\alpha$, respectively, is evident. This corresponds to the planes that are parallel according to the Pitsch OR. Fig. 3(*c*) shows the $(001)_\gamma$ and $(011)_\gamma$ pole figures, including all possible product-phase orientations based on the Pitsch model, calculated from the 32 parent-phase orientations. According to these figures, a major texture intensity can be expected at certain zones of the pole figures. This is a consequence of the preferred orientations of the parent-phase grains due to the hot-rolling process.

Fig. 4(*a*) presents $(111)_\alpha$, $(011)_\alpha$ and $(112)_\alpha$ pole figures showing the average crystal orientation measured by EBSD of one parent phase, corresponding to b.c.c. grain 1 shown in Fig. 3. These pole figures can be compared with the $(011)_\gamma$, $(001)_\gamma$ and $(011)_\gamma$ pole figures plotted in Fig. 4(*b*), corresponding to the average orientations of three product phases activated inside the b.c.c. grain. It can be observed that, for each martensite variant, there is a pole point in the $(011)_\gamma$, $(001)_\gamma$ and $(011)_\gamma$ pole figures that is very close to a pole point in the $(111)_\alpha$, $(011)_\alpha$ and $(112)_\alpha$ pole figures. These results show that, in this case, a very close Pitsch OR exists between the parent and product phases because the parallelism of planes proposed in this model is almost fulfilled.

In order to analyse the distribution of the orientation measured by EBSD in both phases, 500 points of crystal orientation data of a parent and a product phase were randomly selected to represent the experimental orientation results. These points are plotted in $(001)_\alpha$ and $(001)_\gamma$ pole figures, shown in Fig. 4(*c*). The martensite variant, despite having a low grain orientation spread (GOS = 1.2°), clearly shows a preferentiality in its distribution compared with the strongly isotropic distribution observed in the parent phase. In

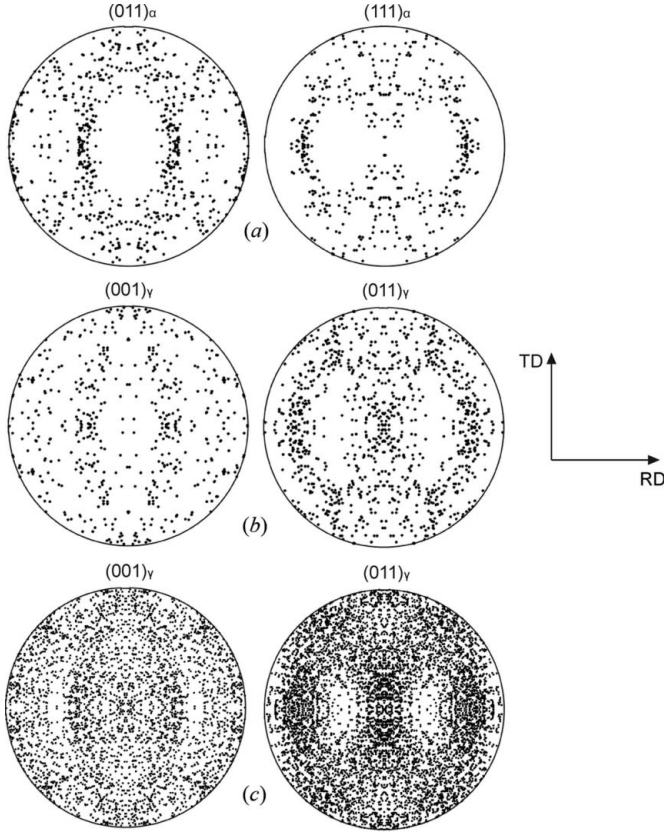

Figure 3
(*a*) $(011)_\alpha$ and $(111)_\alpha$ pole figures showing the average crystal orientations of the 32 parent b.c.c. grains analysed. (*b*) $(001)_\gamma$ and $(011)_\gamma$ pole figures showing the crystal orientations of the 44 product f.c.c. grains. (*c*) $(001)_\gamma$ and $(011)_\gamma$ pole figures showing all possible product-phase orientations based on the Pitsch model.

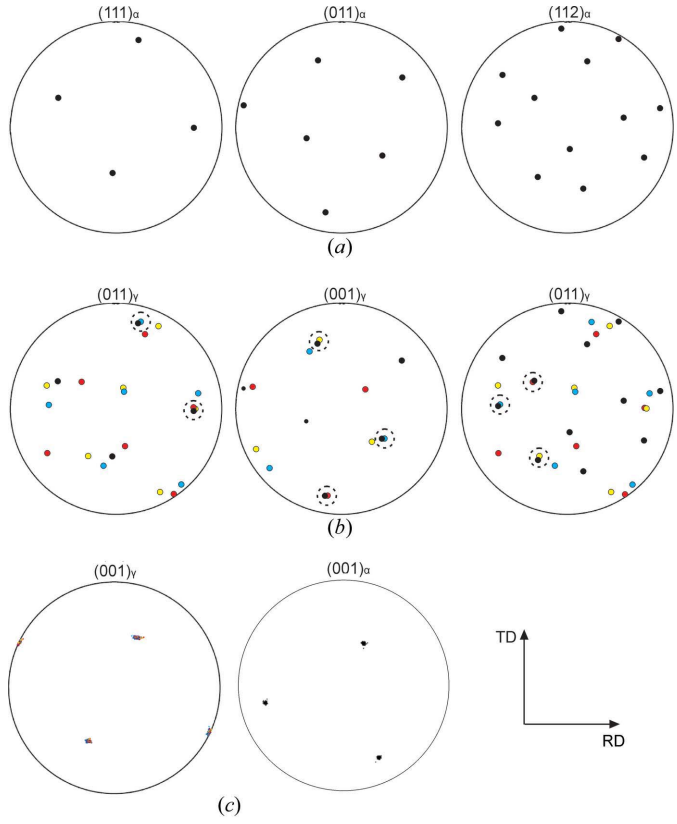

Figure 4
(*a*) $(111)_\alpha$, $(011)_\alpha$ and $(112)_\alpha$ pole figures showing the average crystal orientation measured by EBSD of one parent phase. (*b*) $(011)_\gamma$, $(001)_\gamma$ and $(011)_\gamma$ pole figures corresponding to the average orientations of the three product phases activated inside the b.c.c. grain. Coloured dots correspond to product-phase orientations. Black dots represent the pole points of the b.c.c. orientation plotted in panel (*a*). Dashed circles show α and γ pole points that are coincident. (*c*) $(001)_\alpha$ and $(001)_\gamma$ pole figures showing 500 points of crystal orientation data of a parent-phase grain and a product-phase grain. RD and TD represent the rolling and transverse directions of the sample, respectively.

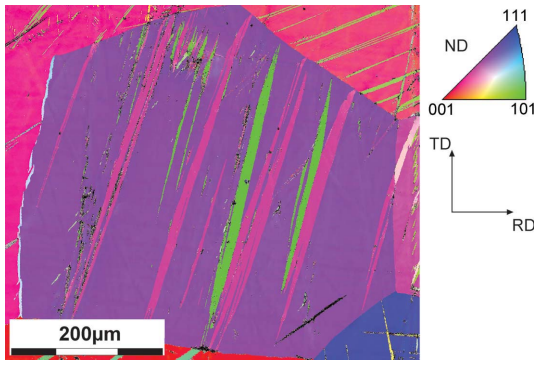

Figure 5
IPF image of b.c.c. grain 4 and two different martensite variants. ND, RD and TD represent the out-of-plane, rolling and transverse directions of the sample, respectively. The step size is 0.07 μm.

terms of isotropy and anisotropy coefficients of the misorientation distribution, the values are 0.18 and 2.08 for the f.c.c. phase and 0.45 and 1.22 for the b.c.c. phase, respectively (Pantleon, 2005). The IPF of these orientations is shown in Fig. 5, where narrow plates corresponding to two different martensite variants can be seen. Some other plates were also observed within this b.c.c. grain, showing a minor development.

Histograms of the misorientation angles are presented in Figs. 6(*a*)–6(*e*). For each ideal OR, the difference between the parent-phase orientation measured by EBSD and the orientation of the closest ideal variant is shown. The most frequent value for the B model is around 9° of misorientation, in agreement with the results obtained by other authors in different materials (Kurdjumow & Sachs, 1930; Nishiyama, 1934; Wassermann, 1935; Pitsch, 1959; Greninger & Troiano, 1949). The most frequent value for the other models oscillates between 6 and 2°. The better correlation is shown by the P OR. A frequency histogram of the OR that provides the best prediction of austenite orientations measured by EBSD is shown in Fig. 6(*f*). The P OR shows the best match in more than 85% of cases. The 15% of cases in which the P OR is not fulfilled are distributed among the KS, GT and B ORs. This can be explained either by the inaccuracy of the technique used or by structural distortions in the microstructure. The latter possibility, which may involve defects in the crystalline lattice, residual stresses due to the quenching process or incompatibilities in grain boundary, could be responsible for the difference in the OR observed in a particular grain. In order to explore this option, we analysed the six cases where the Pitsch relationship was not fulfilled. We found that three of these six cases corresponded to the b.c.c. grain in which four variants of martensite were activated. This grain is shown in Fig. 2 (grain 1). It can be observed that a large fraction of the grain section studied is occupied by wide martensite plates. In contrast, in the grain shown in Fig. 5, narrow martensite plates are observed, occupying a small portion of the analysed surface. In this grain the P OR is fulfilled for the two variants. A morphology of narrow plates allows martensite variants to be accommodated with minor distortions.

Table 3
Correspondence data between the ideal and measured b.c.c. orientations for each OR.

OR	Average misorientation (°)	Standard deviation (°)	Median (°)
B	8.58	1.23	8.72
KS	4.09	0.80	4.12
P	2.35	1.61	2.02
NW	5.96	1.18	6.10
GT	4.34	0.81	4.37

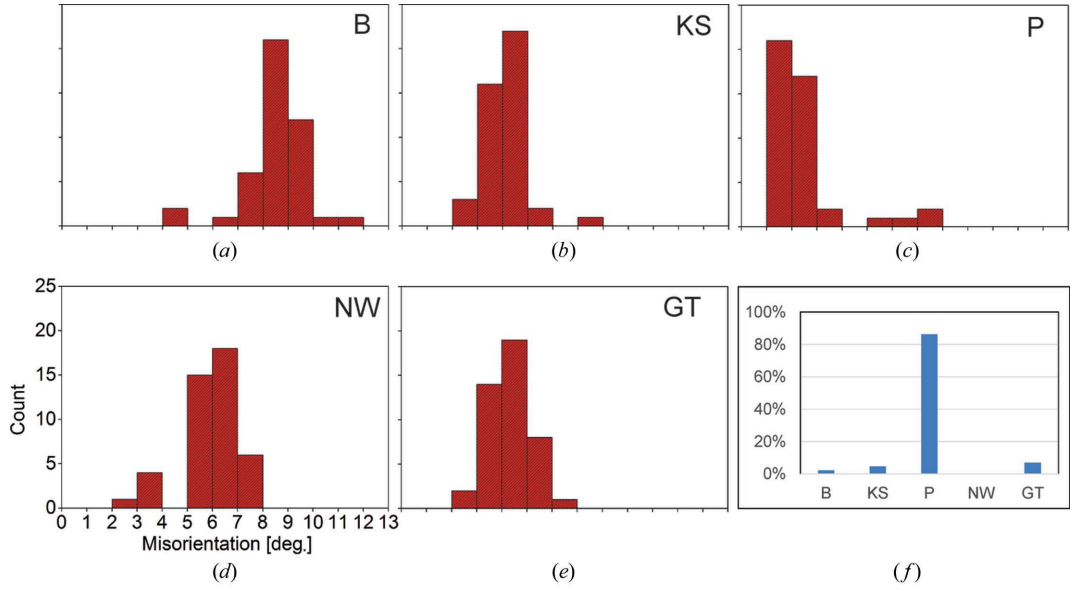

Figure 6
Correspondence between ideal and measured b.c.c. orientations for (*a*) the Bain OR, (*b*) the Kurdjumow–Sachs OR, (*c*) the Pitsch OR, (*d*) the Nishiyama–Wassermann OR and (*e*) the Greninger–Troiano OR. (*f*) A frequency histogram of the ORs that provide the best prediction of austenite orientations measured by EBSD.

It can be seen that all histograms show a sharp peak at certain angles. This could indicate a well defined OR between the parent and product phases in the alloy. The fact that no ideal OR perfectly correlates measured orientations with ideal orientations could be due to two reasons: the inaccuracy of about 1° in the angular resolution of the EBSD technique used, or the lack of an exact f.c.c. structure in the product phase (it may be distorted in such a manner that its angles may deviate slightly from 90°). The latter option is supported by TEM studies carried out by Omori *et al.* (2012). Despite this, according to the experimental results, the P model represents the OR between the orientations of the austenite and martensite in the FMAN system in an acceptable way. Moreover, in the light of these observations, it is worth noting that our results provide experimental support to a theoretical model of the transformation in these FMAN alloys proposed recently by Ojha & Sehitoglu (2016). The correspondence data of each model are summarized in Table 3.

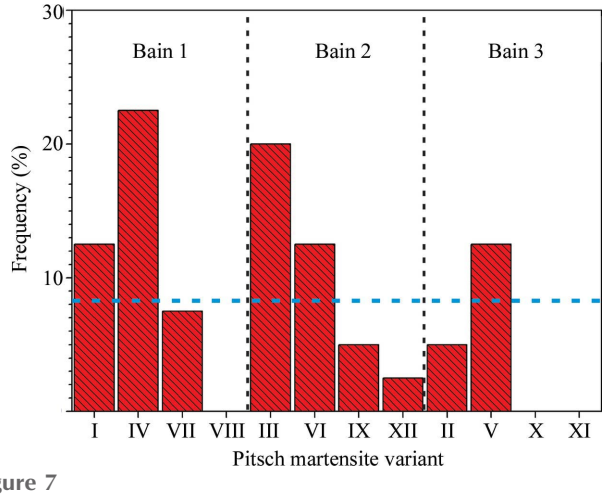

Figure 7
The global distribution of the different variants activated for the Pitsch OR. The horizontal dashed line represents the frequency for a random distribution.

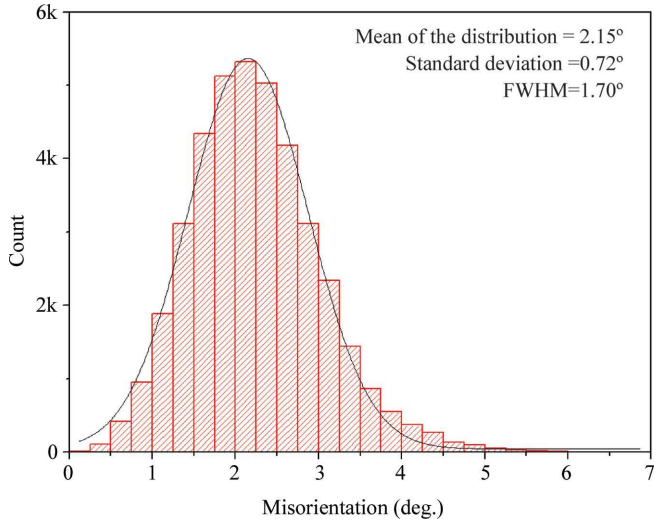

Figure 8
A histogram of misorientation angles between 200 random measured f.c.c. orientations transformed by the best Pitsch rotation matrix and 200 b.c.c. orientations measured by EBSD for b.c.c. grain number 2.

Table 4
OR corresponding to each variant for the Pitsch and Bain models.

Bain variant	Pitsch variant	$\{001\}_\gamma \parallel \{110\}_\alpha$	$\langle 110\rangle_\gamma \parallel \langle 111\rangle_\alpha$
1,	1	$(001)_\gamma \parallel (011)_\alpha$	$[\bar{1}10]_\gamma \parallel [\bar{1}1\bar{1}]_\alpha$
$(100)_\gamma \parallel (100)_\alpha$,	4	$(010)_\gamma \parallel (011)_\alpha$	$[\bar{1}01]_\gamma \parallel [\bar{1}11]_\alpha$
$[010]_\gamma \parallel [011]_\alpha$	7	$(001)_\gamma \parallel (011)_\alpha$	$[110]_\gamma \parallel [11\bar{1}]_\alpha$
	8	$(010)_\gamma \parallel (011)_\alpha$	$[101]_\gamma \parallel [1\bar{1}1]_\alpha$
2,	3	$(100)_\gamma \parallel (101)_\alpha$	$[0\bar{1}1]_\gamma \parallel [\bar{1}11]_\alpha$
$(010)_\gamma \parallel (010)_\alpha$,	6	$(001)_\gamma \parallel (101)_\alpha$	$[\bar{1}10]_\gamma \parallel [\bar{1}11]_\alpha$
$[001]_\gamma \parallel [101]_\alpha$	9	$(001)_\gamma \parallel (\bar{1}01)_\alpha$	$[110]_\gamma \parallel [111]_\alpha$
	12	$(100)_\gamma \parallel (101)_\alpha$	$[011]_\gamma \parallel [\bar{1}11]_\alpha$
3,	2	$(100)_\gamma \parallel (110)_\alpha$	$[0\bar{1}1]_\gamma \parallel [1\bar{1}1]_\alpha$
$(001)_\gamma \parallel (001)_\alpha$,	5	$(010)_\gamma \parallel (\bar{1}10)_\alpha$	$[\bar{1}01]_\gamma \parallel [\bar{1}11]_\alpha$
$[100]_\gamma \parallel [110]_\alpha$	10	$(010)_\gamma \parallel (\bar{1}10)_\alpha$	$[101]_\gamma \parallel [111]_\alpha$
	11	$(100)_\gamma \parallel (1\bar{1}0)_\alpha$	$[011]_\gamma \parallel [111]_\alpha$

Fig. 7 shows the distribution of the different variants activated for the Pitsch OR. The horizontal dashed line represents the frequency for a random distribution. The Pitsch variants were gathered into three groups, considering those that are close to each of the three Bain variants in a $\{001\}_\alpha$ pole figure (Verbeken *et al.*, 2009). Despite the absence of an external load during phase transformation, some variants were found more often than the frequency for a random distribution. On the other hand, there are three variants that appear to be missing and some others that are present at a very low frequency. Furthermore, the variants gathered around Bain variant 3 were found at a lower frequency than the variants gathered around the other two. This global variant selection could be attributed to the texture in the b.c.c. parent phase as a consequence of the hot-rolling process. Table 4 summarizes the planes and directions that remain parallel in the α and γ phases for every Pitsch and Bain variant.

Although the average orientations used for the calculations have low values of GOS (less than 1.3° in all cases), a study was carried out to evaluate how data dispersion affects the results obtained. For this purpose, 200 dots of the orientation map measured by EBSD were randomly taken for each product phase. The rotation matrix of every model that produced the closest approximation to the orientation of the measured parent phase was applied to these 200 f.c.c. orientations. Finally, these transformed orientations were compared with 200 dots of the orientation map of the corresponding parent phase obtained by EBSD. Thus, 40 000 misorientation angles were calculated and plotted in histograms. The curves obtained correspond to normal distributions whose standard deviations were less than 1.3°. Furthermore, their medians were very close to those obtained by performing the calculations with mean values for all cases. This indicates that the effect of the input data spread used in this study does not severely affect the results obtained from average values. As an example, one of these histograms of misorientation between the orientations calculated by P and those of the measured parent phase is shown in Fig. 8. The mean of the distribution was 2.15°. On the other hand, the misorientation angle calculated using average orientations was 2.08° for this

example. In this calculation, the EBSD GOSs for the b.c.c. and f.c.c. phases were 0.78 and 0.91°, respectively. This dispersion in the input data is acceptable since the misorientation results calculated for this grain using mean values and random points are very similar.

4. Conclusions

For the first time, the $\alpha \rightarrow \gamma'$ martensitic transformation OR has been well established experimentally. Five different relationships (Bain, Kurdjumow–Sachs, Pitsch, Nishiyama–Wassermann and Greninger–Troiano) were employed to analyse the $Fe_{43.5}Mn_{34}Al_{15}Ni_{7.5}$ (at.%) system and its $\alpha \rightarrow \gamma'$ thermally induced martensitic transformation. The orientations predicted by these relationships were compared with EBSD and the following conclusions can be drawn:

(i) The Pitsch model captures the transformation in more than 85% of the analysed cases. The median of the misorientation between the parent-phase orientation, measured by EBSD, and the orientation of the closest ideal variant is around 2° for this OR. This result is consistent with the dislocation-based heterogeneous Bogers–Burgers type transformation mechanism, recently proposed by Ojha & Sehitoglu (2016).

(ii) A well defined OR may exist between austenite and martensite, since very high peaks are observed at particular angles in the histograms of minimum misorientations for all the models.

(iii) The microstructure's morphological conditions appear to be responsible for differences in the OR between the parent and martensite phases in a particular grain. Narrow martensite plates in b.c.c. grains satisfy the Pitsch OR, whereas in b.c.c. grains with a large volume fraction occupied by wide martensite plates, such a condition has not been completely verified.

(iv) There are some indications of a global variant selection in the thermally activated transformations. This could be attributed to the texture in the parent phase.

Acknowledgements

The authors thank P. Rizzo and V. Tartalini for their technical assistance.

Funding information

The following funding is acknowledged: Consejo Nacional de Investigaciones Científicas y Técnicas (CONICET, Argentina) (grant No. PDTS 251; grant No. PIP 0488; grant No. PUE-IFIR).

References

Ahlers, M. (1986). *Mater. Sci.* **30**, 135–186.
Ando, K., Omori, T., Ohnuma, I., Kainuma, R. & Ishida, K. (2009). *Appl. Phys. Lett.* **95**, 212504.
Bain, E. C. (1924). *Trans. AIME*, **70**, 25–47.
Bogers, A. & Burgers, W. (1964). *Acta Metall.* **12**, 255–261.
Bowles, J. & Mackenzie, J. (1954*a*). *Acta Metall.* **2**, 129–137.
Bowles, J. & Mackenzie, J. (1954*b*). *Acta Metall.* **2**, 224–234.
Cayron, C. (2013). *Acta Cryst.* A**69**, 498–509.
Cayron, C., Barcelo, F. & de Carlan, Y. (2010). *Acta Mater.* **58**, 1395–1402.
Greninger, A. & Troiano, A. (1949). *Trans. AIME*, **185**, 590–598.
He, Y., Godet, S. & Jonas, J. J. (2005). *Acta Mater.* **53**, 1179–1190.
Hielscher, R. & Schaeben, H. (2008). *J. Appl. Cryst.* **41**, 1024–1037.
Koumatos, K. & Muehlemann, A. (2017). *Acta Cryst.* A**73**, 115–123.
Kurdjumow, G. & Sachs, G. (1930). *Z. Phys.* **64**, 325–343.
Mackenzie, J. & Bowles, J. (1954). *Acta Metall.* **2**, 138–147.
Nishiyama, Z. (1934). *Sci. Rep. Tohoku Imp. Univ.* **23**, 637–642.
Nishiyama, Z. (1978). *Martensitic Transformation.* Oxford: Elsevier Science.
Nolze, G. (2004). *Z. Metallkd.* **95**, 744–755.
Ojha, A. & Sehitoglu, H. (2016). *Int. J. Plast.* **86**, 93–111.
Omori, T., Ando, K., Okano, M., Xu, X., Tanaka, Y., Ohnuma, I., Kainuma, R. & Ishida, K. (2011). *Science*, **333**, 68–71.
Omori, T., Nagasako, M., Okano, M., Endo, K. & Kainuma, R. (2012). *Phys. Lett.* **101**, 231907.
Otsuka, K. (2002). *Shape Memory Materials.* Cambridge University Press.
Pantleon, W. (2005). *Mater. Sci. Technol.* **21**, 1392–1396.
Pitsch, W. (1959). *Philos. Mag.* **4**, 577–584.
Pitsch, W. (1962). *Acta Metall.* **10**, 79–80.
Roitburd, A. & Kurdjumov, G. (1979). *Mater. Sci. Eng.* **39**, 141–167.
Sandoval, L. M., Urbassek, H. & Entel, P. (2009). *New J. Phys.* **11**, 103027.
Sato, A., Chishima, E., Soma, K. & Mori, T. (1982). *Acta Metall.* **30**, 1177–1183.
Sehitoglu, H., Karaman, I., Zhang, X., Chumlyakov, Y. & Maier, H. (2001). *Scr. Mater.* **44**, 779–784.
Sinclair, C. & Hoagland, R. (2008). *Acta Mater.* **56**, 4160–4171.
Sure, G. N. & Brown, C. (1984). *Metall. Mater. Trans. A*, **15**, 1613–1621.
Tseng, L., Ma, J., Wang, S., Karaman, I. & Chumlyakov, Y. (2016). *Scr. Mater.* **116**, 147–151.
Tseng, L., Ma, J., Wang, S., Karaman, I., Kaya, M., Luo, Z. P. & Chumlyakov, Y. I. (2015). *Acta Mater.* **89**, 374–383.
Umino, R., Liu, X., Sutou, Y., Wang, C., Ohnuma, I., Kainuma, R. & Ishida, K. (2006). *J. Phase Equilibria Diffusion*, **27**, 54–62.
Verbeken, K., Barbé, L. & Raabe, D. (2009). *ISIJ Int.* **49**, 1601–1609.
Vollmer, M., KrooB, P., Kriegel, M., Klemm, V., Somsen, C., Ozcan, H., Karaman, I., Weidner, A., Rafaja, D., Biermann, H. & Niendorf, T. (2016). *Scr. Mater.* **114**, 156–160.
Wassermann, G. (1935). *Mitt. Kaiser-Wilhelm-Inst. Eisenforsch. Düsseldorf*, **17**, 149–155.
Wechsler, M., Lieberman, D. & Read, T. (1953). *J. Metals*, **197**, 1503–1515.
Yang, X., Sun, S., Wu, X., Ma, E. & Zhang, T. (2014). *Sci. Rep.* **4**, 6141.